Journal of Photochemistry and Photobiology A: Chemistry 218 (2011) 69–75

Contents lists available at ScienceDirect

Journal of Photochemistry and Photobiology A: Chemistry

journal homepage: www.elsevier.com/locate/jphotochem

Kinetic studies of emissive guanine derivatives bearing anthracene moiety

Yoshinobu Nishimura, Koki Shimamura, Yo Ohmori, Yoshihiro Shinohara, Tatsuo Arai*

Graduate School of Pure and Applied Sciences, University of Tsukuba, Tsukuba, Ibaraki 305-8571, Japan

ARTICLE INFO

Article history:
Received 4 August 2010
Received in revised form 3 December 2010
Accepted 8 December 2010
Available online 16 December 2010

Keywords:
Photoinduced electron transfer
Guanine
Anthracene
Exciplex emission
Fluorescence decay
Kinetic analysis

ABSTRACT

Photoirradiation of methylene-linked anthracene-guanine compounds, which are substituted at the 2 and 9 positions of the anthracene moiety, showed locally excited emission (LE) as well as intramolecular exciplex emission as a result of quenching of the excited singlet state of the anthracene moiety by the guanine moiety. This was confirmed by time-resolved fluorescence as well as steady-state spectroscopy and provides another approach for detecting base-pair formation. Quenching processes by the guanine moiety were investigated by the assumption of equilibrium in the excited state leading to a consistent explanation of the quenching ratio of LE. The quenching rate constant of the excited anthracene moiety by the guanine moiety mainly depends on the intrinsic reduction potential of the anthracene moiety.

1. Introduction

Recently there has been considerable fundamental and practical interest in the photoreaction of DNA like an appropriate photocleavage agent for initiating cleavage of the target nucleic acid [1,2]. Much effort was devoted to elucidate the mechanism of oxidative reaction of nucleobases with photosensitizers [3–8]. Guanine is well known to undergo photodamage by singlet oxygen or photoadduct formation through the excited state of a photosensitizer [9–11]. Some resulting holes in DNA strands are allowed to hop via a guanine moiety and get trapped in cytosine or thymine sites followed by the formation of oxidized products.

The aim of the present work is to explore the dynamics of the excited state associated with a guanine derivative including time constants involved. However, guanine, the most electron-donating of the nucleobases, exhibits a very short excited singlet state leading to very few emissions in the ultraviolet region as well as difficulty in detection by fluorescence measurements [12–14]. The development of emissive species associated with guanine provides another approach to detect base-pair formation. Subsequent utilization of well-developed techniques including steady state and transient measurements may allow the investigation of dynamic motions of targeted proteins [1,15].

Guanine linked to pyrene, **PyG**, has been reported to show new emission as well as locally excited emission associated with the pyrene moiety [16,17]. This new emission is attributed to exciplex emission preceded by the quenching of the excited singlet state of the pyrene moiety by the guanine moiety. Although the qualitative properties of guanine–pyrene compounds have been investigated in earlier reports, the details of kinetics in the excited state still are unknown. Since pyrene is known to form an excimer, which causes difficulty in investigations of dynamics, anthracene was chosen as a sensitizer due to the rarity of its excimer formation. Time-resolved fluorescence measurements, which allow the estimation of rate constants involved in the excited state, were performed to investigate the formation and relaxation processes of exciplex and locally excited state of the anthracene moiety (LE). Two different guanine derivatives connected to 2 and 9 positions of anthracene, hereafter referred to as **An-2-G** and **An-9-G**, respectively, were prepared to study free energy changes involved in the electron transfer reaction. Both **An-2-G** and **An-9-G** showed exciplex emission in toluene solution containing 10 vol.% of *N*,*N*-dimethylformamide (DMF), while no exciplex emission was observed in DMF due to the promotion of subsequent reactions such as charge separation [18–32]. In general, a fixed geometry of the donor–acceptor system is required to investigate the kinetics of photoreaction in the excited state due to easy estimation of geometric parameters such as distance and orientation involved in the donor–acceptor reaction. However, a flexible linker system would offer advantages for potential various geometries, which allow more conformation and a wider range of environments to be detected in comparison with rigid donor–acceptor systems [33,34]. For this reason, a methylene chain was chosen as the linker, although rigid donor–acceptor systems should not be eliminated as sensors.

As found in pyrene excimer kinetics studied by Birks, it was assumed that there was an equilibrium between the LE and exciplex

* Corresponding author.
E-mail address: arai@chem.tsukuba.ac.jp (T. Arai).

1010-6030/$ – see front matter © 2010 Published by Elsevier B.V.
doi:10.1016/j.jphotochem.2010.12.005

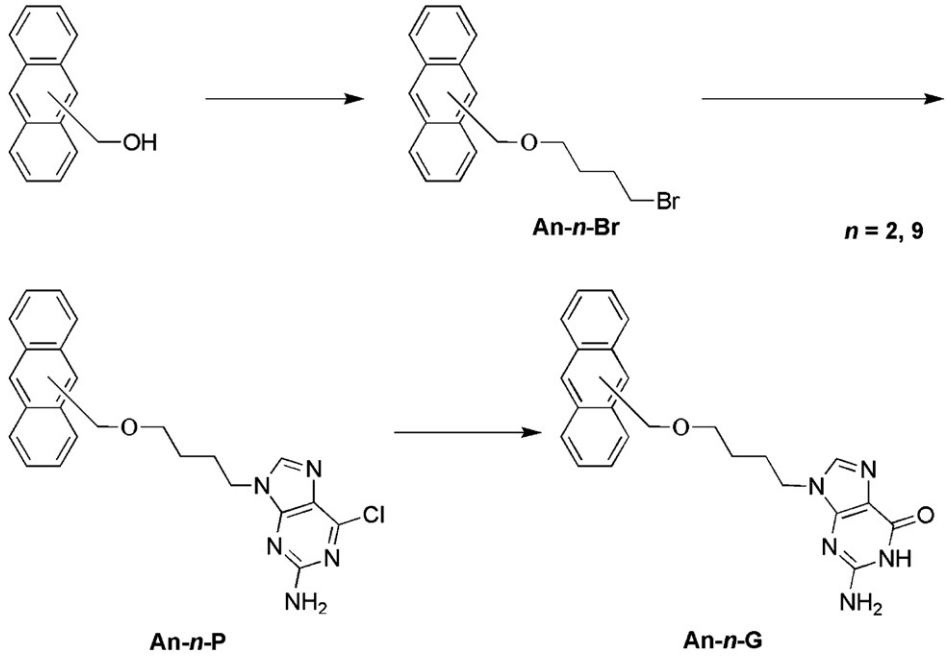

Scheme 1.

since the decay curves exhibited a bi-exponential profile. Longer lifetimes of LE and exciplex were in good agreement with each other [35]. Theoretical population decay according to Birks enabled the determination of forward and backward electron transfer rate constants, k_{CS} and k_{-CS}, between LE and exciplex. It was found that k_{CS} is mainly dependent on the free energy change between the initial and final states in the photoinduced electron transfer reaction.

2. Experimental

2.1. Instruments

Absorption and fluorescence spectra were measured using Shimadzu UV-1600 and on Hitachi F-4500 fluorescence spectrometers, respectively. Fluorescence decay measurement was performed by using the time-correlated single-photon counting method with excitation of 375 nm, which was achieved by using a diode laser (PicoQuant, LDH-P-C-375) with a power control unit (PicoQuant, PDL 800-B) in a repetition rate of 2.5 MHz [36,37]. Differential pulse voltammetric measurement was carried out by CV-50W Voltammetric analyzer (BAS) with an Ag/AgCl reference electrode. ^{1}H and ^{13}C NMR spectra were measured by using a 400-MHz NMR spectrometer (ARX-400, Bruker). ESI-mass spectra were acquired by API QSTAR pulsar i (Applied Biosystems/MDS SCIEX). Solvent used in spectroscopic measurement was toluene containing 10 vol.% of *N*,*N*-dimethylformamide (DMF) due to the limited solubility of samples in toluene. Fluorescence quantum yields were estimated by using anthracene as a reference compound (Φ_F = 0.27 in ethanol).

3. Materials

Samples were prepared as shown in Scheme 1. See also Supporting Information (Figs. S7–S15).

Synthesis of An-9-Br. Anthracene-9-methanol (1.11 g, 5.35 mmol) and 1,4-dibromobutane (2.46 g, 11.4 mmol) were stirred in dry THF (20 ml) at 70 °C. After adding NaH (50%, 0.58 g, 12 mmol) to this mixture, the mixture was refluxed for 4 h at 100 °C under N_2.

The crude product was dissolved in water (30 ml) and extracted with diethylether (50 ml, 3×). The organic phase was dried over anhydrous $MgSO_4$, and the solvent was evaporated under reduced pressure. The residue was purified by silica gel chromatography (eluent:hexane-EtOAc = 10:1) to yield **An-9-Br** (641 mg, 1.87 mmol, 34.9% yield): ^{1}H NMR ($CDCl_3$, 400 MHz) δ 8.41 (s, 1H, An-10), 8.33 (d, J = 8.8 Hz, 2H, An-1,8 or An-4,5), 7.97 (d, J = 8.4 Hz, 2H, An-4,5 or An-1,8), 7.51 (dd, J = 8.8, 6.6 Hz, 2H, An-2,7 or An-3,6), 7.44 (dd, J = 8.4, 6.6 Hz, 2H, An-3,6 or An-2,7), 5.41 (s, 2H, An–CH_2), 3.63 (t, J = 6.2 Hz, 2H, O–CH_2– or –CH_2–Br), 3.31 (t, J = 6.6 Hz, 2H, –CH_2–Br or O–CH_2–), 1.88 (tt, J = 7.4, 6.6 Hz, 2H, –CH_2–CH_2Br or OCH_2–CH_2–), 1.73 (tt, J = 7.4, 6.2 Hz, 2H, OCH_2–CH_2– or –CH_2–CH_2Br); ^{13}C NMR ($CDCl_3$, 100 MHz) δ 131.4, 130.9, 129.0, 128.7, 128.3, 126.1, 124.9, 124.2, 69.3, 64.9, 33.7, 29.6, 28.4.

Synthesis of An-9-P. A mixture of **An-9-Br** (640 mg, 1.86 mmol), K_2CO_3 (439 mg, 3.18 mmol), TBAI (69.0 mg, 0.187 mmol), and 2-amino-6-chloropurine (268 mg, 1.58 mmol) in DMF (40 ml) was stirred for 15 h at 80 °C under N_2. After adding CH_2Cl_2 (60 ml) to this mixture, the mixture was washed with water (30 ml, 10×). The organic phase was dried over anhydrous $MgSO_4$, and the solvent was evaporated under reduced pressure. The residue was purified by silica gel chromatography (eluent:CH_3Cl–EtOAc = 2:1) to yield **An-9-P** (336 mg, 0.778 mmol, 49.2% yield): ^{1}H NMR ($CDCl_3$, 400 MHz) δ 8.46 (s, 1H, An-10), 8.36 (d, J = 8.8 Hz, 2H, An-1,8 or An-4,5), 8.01 (d, J = 8.4 Hz, 2H, An-4,5 or An-1,8), 7.53 (dd, J = 8.8, 6.5 Hz, 2H, An-2,7 or An-3,6), 7.48 (s, 1H, Purine-8), 7.47 (dd, J = 8.5, 6.5 Hz, 2H, An-3,6 or An-2,7), 5.48 (s, 2H, An–CH_2), 5.04 (s, 2H, Purine–NH_2), 3.90 (t, J = 7.4 Hz, 2H, –CH_2–N or O–CH_2–), 3.68 (t, J = 5.9 Hz, 2H, O–CH_2– or –CH_2–N), 1.86 (tt, J = 7.4, 7.3 Hz, 2H, –CH_2–CH_2N or OCH_2–CH_2–), 1.60 (tt, J = 7.3, 5.9 Hz, 2H, OCH_2–CH_2– or –CH_2–CH_2N); ^{13}C NMR ($CDCl_3$, 100 MHz) δ 158.9, 153.7, 151.1, 142.4, 131.4, 130.9, 129.1, 128.7, 128.4, 126.2, 125.3, 125.0, 124.1, 69.4, 65.0, 43.4, 26.8, 26.7.

Synthesis of An-9-G. Aqueous 0.33 N NaOH (15 ml) was added to a stirring solution of **An-9-P** (336 mg, 0.778 mmol) in 1,4-dioxane (30 ml) and refluxed for 3 h at 120 °C under N_2. This mixture was cooled to room temperature and acidified to pH 4 with 1 N HCl. After adding water (300 ml) to this mixture, the organic phase was evaporated under reduced pressure. The residue was puri-

fied by silica gel chromatography (eluent:CH_3Cl–MeOH = 50:1) to yield **An-9-G** (84.8 mg, 0.205 mmol, 26.3% yield): ^{1}H NMR (DMF-d_7, 400 MHz) δ 10.49 (br s, 1H, Purine-1), 8.65 (s, 1H, An-10), 8.48 (d, J = 8.4 Hz, 2H, An-1,8 or An-4,5), 8.13 (d, J = 7.9 Hz, 2H, An-4,5 or An-1,8), 7.66 (s, 1H, Purine-8), 7.60 (dd, J = 8.4, 6.9 Hz, 2H, An-2,7 or An-3,6), 7.54 (dd, J = 7.9, 6.9 Hz, 2H, An-3,6 or An-2,7), 6.56 (s, 2H, Purine–NH_2), 5.50 (s, 2H, An–CH_2), 4.02 (t, J = 6.9 Hz, 2H, –CH_2–N or O–CH_2–), 3.77 (t, J = 6.1 Hz, 2H, O–CH_2– or –CH_2–N), 1.86 (tt, J = 7.6, 6.9 Hz, 2H, –CH_2–CH_2N or OCH_2–CH_2–), 1.60 (tt, J = 7.6, 6.1 Hz, 2H, OCH_2–CH_2– or –CH_2–CH_2N); ^{13}C NMR ($CDCl_3$, 100 MHz) δ 162.9, 157.7, 154.6, 152.2, 137.9, 132.1, 131.5, 130.3, 129.6, 128.7, 126.8, 125.8, 125.3, 70.4, 65.1, 43.2, 27.6, 27.5; ESI-MS calcd. for $C_{23}H_{24}N_5O_2$ $[M+H]^+$ = 414.19 found: 414.19.

Synthesis of An-2-Br. Anthracene-2-methanol (54.6%, 2.54 g, 6.65 mmol), which was prepared according to Babudri et al. [38], and 1,4-dibromobutane (3.12 g, 14.5 mmol) were stirred in dry THF (90 ml) at 0 °C. After adding NaH (50%, 1.79 g, 38 mmol) to this mixture, the mixture was refluxed for 9 h at 74 °C under N_2. The crude product was dissolved in water (200 ml) and extracted with ethyl acetate (100 ml, 5×) and washed by water (100 ml, 3×). The organic phase was dried over anhydrous $MgSO_4$, and the solvent was evaporated under reduced pressure. The residue was purified twice by silica gel chromatography (eluent:hexane-EtOAc = 10:1) to yield **An-2-Br** (550 mg, 1.60 mmol, 24% yield): ^{1}H NMR ($CDCl_3$, 400 MHz) δ 8.40 (s, 1H, An-9 or -10), 8.39 (s, 1H, An-10 or -9), 8.01–7.97 (m, 3H, An-4,5,8), 7.90 (s, 1H, An-1), 7.47–7.41 (m, 3H, An-3,6,7), 4.68 (s, 2H, An–CH_2), 3.57 (t, J = 6.1 Hz, 2H, O–CH_2– or –CH_2–Br), 3.45 (t, J = 6.6 Hz, 2H, –CH_2–Br or O–CH_2–), 2.01 (tt, J = 7.5, 6.6 Hz, 2H, –CH_2–CH_2Br or OCH_2–CH_2–), 1.80 (tt, J = 7.5, 6.1 Hz, 2H, OCH_2–CH_2– or –CH_2–CH_2Br); ^{13}C NMR ($CDCl_3$, 100 MHz) δ 135.3, 131.9, 131.7, 131.4, 131.2, 128.5, 128.2, 128.1, 126.2 (2Carbon), 126.1, 125.41, 125.37, 125.3, 73.1, 69.3, 33.8, 29.7, 28.4.

Synthesis of An-2-P. A mixture of An-2-Br (253 mg, 0.736 mmol), K_2CO_3 (198 mg, 1.43 mmol), TBAI (27.0 mg, 0.0731 mmol), and 2-amino-6-chloropurine (103 mg, 0.604 mmol) in DMF (45 ml) was stirred for 26 h at 80 °C under N_2. This mixture solution was poured into water (50 ml), producing to a yellowish precipitate, washed with water (100 ml) and dried in vacuo. This procedure afforded crude solid (272 mg). The residue was purified by silica gel chromatography (eluent:EtOAc-hexane = 1:1) to yield **An-2-P** (167 mg, 0.386 mmol, 64% yield): ^{1}H NMR ($CDCl_3$, 400 MHz) δ 8.40 (s, 1H, An-9 or -10), 8.39 (s, 1H, An-10 or -9), 8.01–7.97 (m, 3H, An-4,5,8), 7.90 (s, 1H, An-1), 7.76 (s, 1H, Purine-8), 7.49–7.41 (m, 3H, An-3,6,7), 5.03 (s, 2H, Purine–NH_2), 4.68 (s, 2H, An–CH_2), 4.12 (t, J = 7.2 Hz, 2H, –CH_2–N or O–CH_2–), 3.58 (t, J = 6.1 Hz, 2H, O–CH_2– or –CH_2–N), 2.01 (tt, J = 7.5, 7.2 Hz, 2H, –CH_2–CH_2N or OCH_2–CH_2–), 1.68 (tt, J = 7.5, 6.1 Hz, 2H, OCH_2–CH_2– or –CH_2–CH_2N); ^{13}C NMR ($CDCl_3$, 100 MHz) δ 159.0, 153.7, 151.0, 142.3, 135.0, 131.7, 131.6, 131.2, 131.1, 128.5, 128.1, 128.0, 126.2, 126.03, 126.0, 125.4, 125.31, 125.28, 125.1, 73.2, 69.3, 43.5, 26.8, 26.7.

Synthesis of An-2-G. Aqueous 0.33 N NaOH (10 ml) was added to a stirring solution of An-2-P (167 mg, 0.387 mmol) in 1,4-dioxane (20 ml) and refluxed for 3 h at 120 °C under N_2. This mixture was cooled to room temperature and acidified to pH 4 with 1 N HCl. The product was extracted with ethyl acetate. The residue was purified by silica gel chromatography (eluent:CH_3Cl–MeOH = 12:1) to yield **An-2-G** (21.6 mg, 0.0522 mmol, 13.5% yield): ^{1}H NMR (DMF-d_7, 400 MHz) δ 10.67 (brs, 1H, Purine-1), 8.58 (s, 2H, An-9,10), 8.13–8.08 (m, 3H, An-4,5,8), 8.02 (s, 1H, An-1), 7.77 (s, 1H, Purine-8), 7.55–7.48 (m, 3H, An-3,6,7), 6.63 (s, 2H, Purine–NH_2), 4.69 (s, 2H, An–CH_2), 4.09 (t, J = 6.9 Hz, 2H, –CH_2–N or O–CH_2–), 3.60 (t, J = 6.4 Hz, 2H, O–CH_2– or –CH_2–N), 1.95 (tt, J = 7.7, 6.9 Hz, 2H, –CH_2–CH_2N or OCH_2–CH_2–), 1.64 (tt, J = 7.7, 6.4 Hz, 2H, OCH_2–CH_2– or –CH_2–CH_2N); ^{13}C NMR ($CDCl_3$, 100 MHz) δ 162.9, 157.8, 154.7, 152.3, 138.1, 136.9, 132.6, 132.4, 132.2, 131.9, 129.0, 128.80, 128.75, 126.74, 126.66, 126.4, 126.2, 126.1, 118.0, 73.1, 70.3, 43.4, 27.5, 27.4; ESI-MS calcd. for $C_{23}H_{24}N_5O_2$ $[M+H]^+$ = 414.19 found: 414.19.

Synthesis of An-9-OMe. Anthracene-9-methanol (108 mg, 0.520 mmol) and NaH (50%, 272 mg, 5.67 mmol) were stirred in dry THF (3 ml) at 0 °C under N_2. After adding methyl iodide (1 mg, 7 mmol) to this mixture, the mixture was stirred for 1 h at 80 °C under N_2. Water was added to this mixture at 0 °C. The product was extracted with diethylether (50 ml, 2×), washed by brine solution and dried over anhydrous $MgSO_4$. The solvent was evaporated under reduced pressure. The residue was purified by silica gel chromatography (eluent:hexane-EtOAc = 9:1) and recrystallization to yield **An-9-OMe** (41.0 mg, 0.18 mmol, 35.5% yield): ^{1}H NMR ($CDCl_3$, 400 MHz) δ 8.48 (s, 1H, An-10), 8.40 (d, J = 8.8 Hz, 2H, An-1,8 or An-4,5), 8.03 (d, J = 8.5 Hz, 2H, An-4,5 or An-1,8), 7.57 (dd, J = 8.8, 6.5 Hz, 2H, An-2,7 or An-3,6), 7.49 (dd, J = 8.5, 6.5 Hz, 2H, An-3,6 or An-2,7), 5.46 (s, 2H, An-CH_2), 3.57 (t, J = 6.2 Hz, 3H, O-CH_3); ^{13}C NMR ($CDCl_3$, 100 MHz) δ 131.4, 131.0, 129.0, 128.6, 128.4, 126.2, 124.9, 124.2, 66.6, 58.4.

Synthesis of An-2-OMe. The same procedure as **An-9-OMe** was performed with anthracene-2-methanol (110 mg, 0.526 mmol), producing **An-2-OMe** (84.0 mg, 0.38 mmol, 72%).

^{1}H NMR ($CDCl_3$, 400 MHz) δ 8.43 (s, 1H, An-9 or -10), 8.42 (s, 1H, An-10 or -9), 8.03–8.00 (m, 3H, An-4,5,8), 8.00 (s, 1H, An-1), 7.49–7.44 (m, 3H, An-3,6,7), 4.67 (s, 2H, An-CH_2), 3.48 (s, 3H, O-CH_3); ^{13}C NMR ($CDCl_3$, 100 MHz) δ 135.1, 131.8, 131.7, 131.4, 131.2, 128.5, 128.2, 128.1, 126.3, 126.2, 126.1, 125.4, 125.3, 74.9, 58.2.

4. Results and discussion

4.1. Steady state spectra

Fig. 1 shows absorption spectra of **An-2-G** and **An-9-G** in toluene solution containing 10 vol.% of DMF. To elucidate the interaction in the ground state, reference compounds corresponding to **An-2-G** and **An-9-G** were prepared, referred to as **An-2-OMe** and **An-9-OMe**, respectively. **An-2-G** shows vibrational structures characteristic of derivatives substituted at the 2-position, reflecting their electronic state as shown in Fig. 1(a) [39–42]. Since **An-2-G** agrees well with its reference compound, the guanine moiety does not seem to affect the electronic state of the anthracene moiety even if those moieties are close proximity to each other, as in the pyrene derivative [16,17]. The distance between the anthracene and guanine moieties also explains the lack of interaction in the ground state due to the long alkyl bridge. As shown in Fig. 1(b), the absorption spectrum of **An-9-G** exhibits nearly the same behavior as that of **An-2-G**. The interaction between the anthracene and guanine moieties of **An-9-G** is negligible in the ground state. In other words, both moieties of **An-2-G** and **An-9-G** have no interaction through the linker, a common feature found in various dyads if the electron transfer reaction is endothermic.

Fluorescence spectra of **An-2-G** and **An-2-OMe** are shown in Fig. 2(a). The intensity of each emission spectrum was normalized by the absorbance at the excitation wavelength. Fig. 2(a) shows the fluorescence spectrum of **An-2-OMe**, which undergoes no intramolecular quenching due to the absence of the guanine moiety. The fluorescence spectral shape of **An-2-OMe** showed typical progression referred to as LE emission. In contrast, the fluorescence spectrum of **An-2-G** shows a decrease in the intensity compared to that of **An-2-OMe**, indicating that intramolecular quenching takes place by the guanine moiety based on the low concentration of 2×10^{-5} M. The intensity decreased to 65% compared to that of **An-2-OMe**. In addition, a concomitant emission peak appeared at a longer wavelength relative to LE emission. The new band was not vibrational but exhibited a broad structure. This is consistent with **PyG**, which indicates a new emissive state associated with

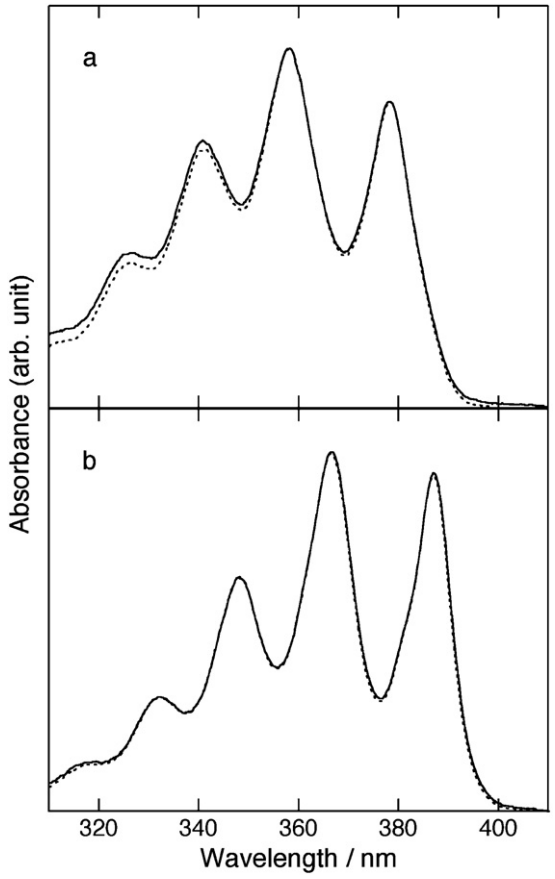

Fig. 1. Absorption spectra of (a) **An-2-G** and (b) **An-9-G** (solid lines) next to their reference compounds **An-2-OMe** and **An-9-OMe** (dashed lines) in toluene containing 10 vol.% of DMF.

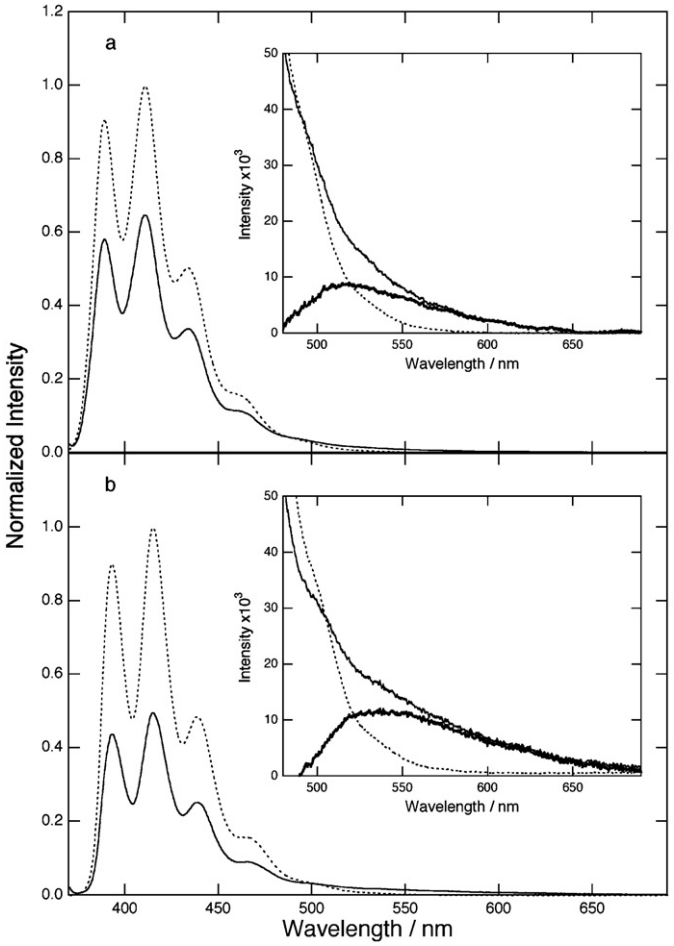

Fig. 2. Fluorescence spectra of (a) **An-2-G** and (b) **An-9-G** (solid lines) next to their reference compounds **An-2-OMe** and **An-9-OMe** (dashed lines) on excitation at 365 nm in toluene containing 10 vol.% of DMF. Subtracted spectrum (bold line) in each inset.

anthracene and guanine moieties was formed. On the other hand, **An-9-G** exhibited a remarkable decrease in intensity of 49% compared to **An-2-G**. **An-9-G** showed a new emission band at a longer wavelength relative to LE, similar to **An-2-G**. Again, these phenomena take place as a result of an intramolecular quenching process, which is responsible for the formation of new bands, considering the relatively low concentration.

Subtraction of the fluorescence spectra of reference compounds from **An-2-G** and **An-9-G** was performed to investigate properties of new bands. The resulting spectra were shown in the inset of Fig. 2. The peak wavelength of **An-2-G** and **An-9-G** were 517 nm and 536 nm, respectively. The energy difference between **An-2-G** and **An-9-G** was calculated to be 0.1 eV. In addition, fluorescence quantum yields of **An-2-G** were calculated to be 0.11 and 0.002 for LE and a new band, respectively. Those of **An-9-G** were to be 0.079 and 0.003.

Excitation spectra of **An-2-G** and **An-9-G** are shown in Fig. 3. To identify the origin of the new emission band, the excitation spectrum monitored at 650 nm was compared to that at 414 nm, which is attributed to LE emission. These two excitation spectra agreed well in their spectral shape and wavelength regions, indicating that the new emission and LE emission have a common origin. Thus, it is revealed that the quenching of the excited singlet state of the anthracene moiety by the guanine moiety results in the formation of a new emissive state, which is consistent with **PyG** [16,17]. The slight difference between the excitation spectra and the absorption spectra may originate from the limit of spectral correction between the spectrophotometer and spectrofluorometer, since no difference in absorption spectra between **An-2-G** and **An-2-OMe** was observed. The excitation spectra of **An-9-G** gave similar results to that of **An-2-G**.

4.2. Fluorescence decay curves

Fig. 4 depicts fluorescence decay curves of **An-2-G** and **An-9-G** monitored at 414 and 610 nm for LE and the new mission band, respectively. LE decay curves of **An-2-G** and **An-9-G** showed bi-exponential decay functions, while the corresponding new bands consisted of rise and decay behaviors as listed in Table 1. The shorter component of LE agrees well with the rise component observed at 610 nm, indicating LE decay is involved in the formation of the new band. This is consistent with the results of the excitation spectra.

Table 1
Fluorescence lifetimes of **An-2-G** and **An-9-G** and obtained rate constants by iterative simulation.

Sample	λ (nm)	τ (ns)	k_D (s^{-1})	k_{CS} (s^{-1})	k_{-CS} (s^{-1})	k_{CR} (s^{-1})
An-2-G	414	2.1 (0.95) 6.1 (0.05)	3.0×10^8	1.7×10^8	3.0×10^7	1.5×10^8
	610	1.5 (−1.00) 9.4 (1.00)	3.0×10^8	1.9×10^8	1.1×10^8	5.2×10^7
An-9-G	414	1.0 (0.94) 5.4 (0.06)	3.9×10^8	5.3×10^8	6.9×10^7	1.7×10^8
	610	1.0 (−1.00) 4.0 (1.00)	3.9×10^8	5.1×10^8	1.2×10^8	2.3×10^8

Parentheses contain the normalized amplitude of each decay component.

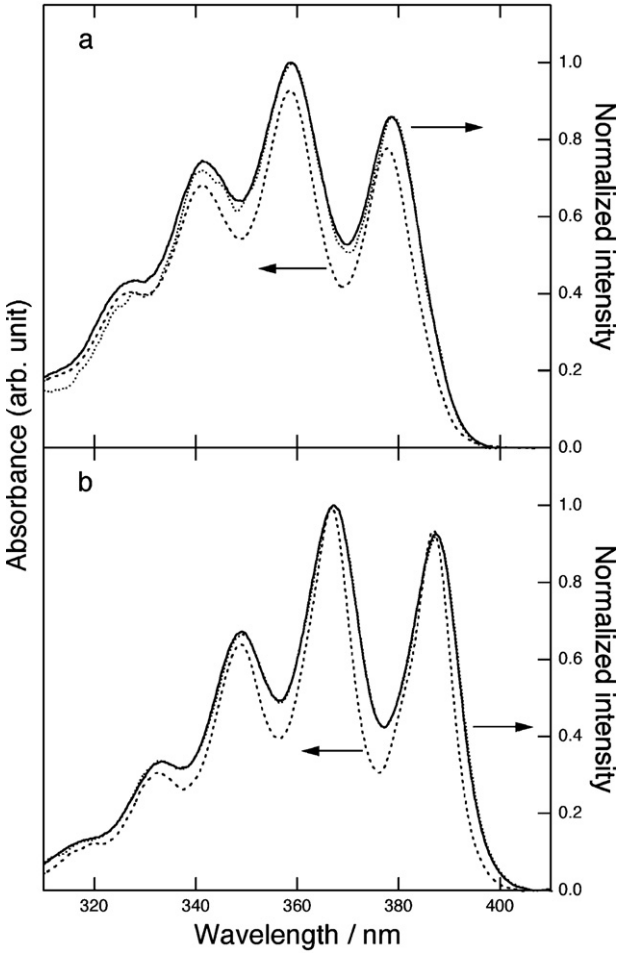

Fig. 3. Fluorescence excitation spectra of (a) **An-2-G** and (b) **An-9-G** monitored at 431 nm (solid line) and 540 nm (dotted line) along with absorption spectrum (dashed line) in toluene containing 10 vol.% of DMF.

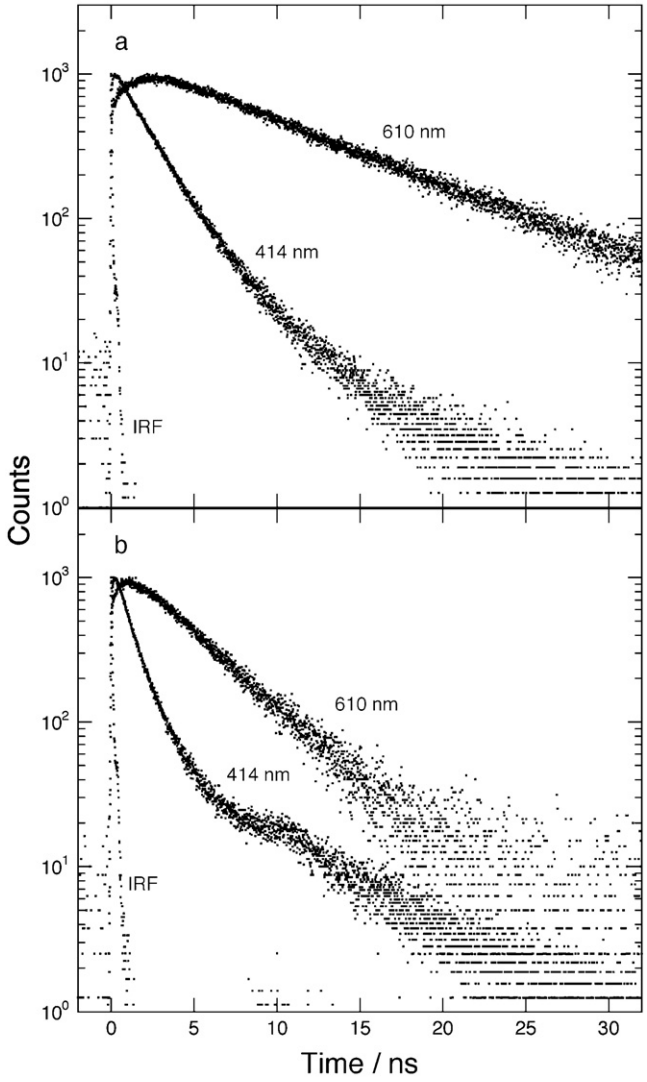

Fig. 4. Fluorescence decay curves of (a) **An-2-G** and (b) **An-9-G** in toluene containing 10 vol.% of DMF observed at 414 nm and 610 nm along with IRF on excitation at 375 nm.

The shorter component may be related to a dynamic process including an encounter between the anthracene and guanine moieties [43]. The time constant corresponding to electron transfer reaction of **An-2-G** was twice of that of **An-9-G**, indicating that quenching of the excited singlet state of the anthracene moiety by the guanine moiety in **An-9-G** seems to be more favorable than in **An-2-G**. This is applicable to the longer component. Thus, a new emission state of **An-2-G** is generated by intramolecular quenching of the excited singlet state of the anthracene moiety by the guanine moiety, followed by slower relaxation, which is confirmed by time-resolved spectra of **An-2-G** and **An-9-G** (see Supporting Information, Figs. S1 and S2, respectively).

4.3. Free energy change

Thermodynamic parameters were estimated by using the redox potentials of **An-2-G** and **An-9-G** and spectroscopic data. In general, the free energy change via the photochemical reaction between an electron donor and an electron acceptor is given as follows:

$$\Delta G = \mathrm{IP_D} - \mathrm{EA_A} - E^*$$

where $\mathrm{IP_D}$, $\mathrm{EA_A}$, and E^* denote the ionization potential of the donor, electron affinity of the acceptor, and S_0–S_1 transition energy, respectively. In the condensed phase, $\mathrm{IP_D}$ and $\mathrm{EA_A}$ are expressed by the oxidation potential ($E^{\mathrm{D}}_{\mathrm{ox}}$) and reduction potential ($E^{\mathrm{A}}_{\mathrm{red}}$), respectively, and can be estimated by differential pulse voltammetry. The free energy change in the electron transfer reaction via the excited state in the condensed phase is given by the following equation:

$$\Delta G_{\mathrm{ET}} = E^{\mathrm{D}}_{\mathrm{ox}} - E^{\mathrm{A}}_{\mathrm{red}} - E^* + C$$

To evaluate the reduction potential of the anthracene moieties of **An-2-G** and **An-9-G**, **An-2-OMe** and **An-9-OMe** were prepared as reference compounds, respectively. Reduction potential values for **An-2-OMe** and **An-9-OMe** were determined to be −2.41 and −2.28 V vs. Ag/AgCl, respectively. The oxidation potential of the guanine moiety was determined to be 0.78 vs. Ag/AgCl (see Supporting Information, Fig. S3). S_0–S_1 transition energies of **An-2-G** and **An-9-G** were determined to be 3.21 and 3.17 eV, respectively, by using the wavenumber where the absorption and emission spectra intersect. If no coulomb term C is considered, free energy changes of **An-2-G** and **An-9-G** were estimated to be −0.02 and −0.11, respectively. Difference of these free energy changes is good agreement with that of peak wavelength of new bands as shown in inset of Fig. 2. Since C was reported to be 0.38 and −0.06 eV for *n*-hexane and acetonitrile, respectively [44], ΔG_{ET} might be almost zero or slightly positive for **An-2-G**, considering the polarity of the solvent used (see Supporting Information, Fig. S4). Photoinduced

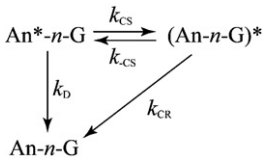

Scheme 2.

electron transfer reactions may proceed under such endothermic conditions [17,45]. These results indicate that electron transfer in **An-9-G** may be more favorable than in **An-2-G** if the reaction occurs in the normal region. Details of electron transfer rates will be discussed later. Thus, the intramolecular reaction taking place in **An-2-G** and **An-9-G** is an electron transfer reaction in the excited singlet state of the anthracene moiety quenched by the guanine moiety, similar to the pyrene–guanine system. Accordingly, the new emission appearing at a longer wavelength relative to LE emission could be attributed to exciplex emission by the comparison to similar compounds [20,43,46].

4.4. Analyses of fluorescence decay

From the above discussion of the kinetics of the exciplex, we propose kinetics involving exciplex formation and deactivation as shown in Scheme 2. When **An-*n*-G** (***n*** = 2, 9) is excited, a locally excited state of the anthracene moiety of **An-*n*-G** is formed, shown as **An*-*n*-G**, followed by the formation of a delocalized excited state, (**An-*n*-G**)*, which is responsible for exciplex emission. The rate constant k_D indicates the deactivation rate constant of **An*-*n*-G** including radiative and nonradiative processes. The formation rate constant of (**An-*n*-G**)* is k_{CS} and its reverse process is k_{-CS}. The deactivation process of (**An-*n*-G**)* to the ground state is k_{CR}, which includes radiative and nonradiative processes of exciplex, as in k_D. If we assume an equilibrium between LE and exciplex as shown in Scheme 2, the following differential equations are given:

$$\frac{d[\mathbf{An^*\text{-}n\text{-}G}]}{dt} = k_{-CS}[(\mathbf{An\text{-}n\text{-}G})^*] - (k_{CS} + k_D)[\mathbf{An^* - n - G}] \quad (1)$$

$$\frac{d[(\mathbf{An\text{-}n\text{-}G})^*]}{dt} = k_{CS}[\mathbf{An^*\text{-}n\text{-}G}] - (k_{-CS} + k_{CR})[(\mathbf{An\text{-}n\text{-}G})^*] \quad (2)$$

where **An*-*n*-G** and (**An-*n*-G**)*Correspond to LE and exciplex, respectively. If we adopt $[\mathbf{An^*\text{-}n\text{-}G}] = [\mathbf{An^*\text{-}n\text{-}G}]_0$ and $[(\mathbf{An\text{-}n\text{-}G})^*]_0 = 0$ at $t = 0$ as the boundary condition, the following solutions are derived [35,47]:

$$\frac{[\mathbf{An^*\text{-}n\text{-}G}]}{[\mathbf{An^*\text{-}n\text{-}G}]_0} = \frac{1}{\gamma_1 - \gamma_2}\{(X - \gamma_2)\exp(-\gamma_1 t) - (X - \gamma_1)\exp(-\gamma_2 t)\} \quad (3)$$

$$\frac{[(\mathbf{An\text{-}n\text{-}G})^*]}{[\mathbf{An^*\text{-}n\text{-}G}]_0} = \frac{k_{CS}}{\gamma_1 - \gamma_2}\{\exp(-\gamma_2 t) - \exp(-\gamma_1 t)\} \quad (4)$$

where

$$\gamma_1 = \frac{1}{2}\{(X + Y) + \sqrt{(X - Y)^2 + 4k_{-CS}k_{CS}}\} \quad (5)$$

$$\gamma_2 = \frac{1}{2}\{(X + Y) - \sqrt{(X - Y)^2 + 4k_{-CS}k_{CS}}\} \quad (6)$$

$$X = k_D + k_{CS}, \quad Y = k_{CR} + k_{-CS} \quad (7)$$

Eqs. (3) and (4) describe the time development of LE emission observed at 414 nm and exciplex at 610 nm, respectively. If $\gamma_1 - \gamma_2 > 0$ from Eqs. (6) and (7), then Eq. (4) shows that the exciplex rises at a rate constant of γ_1 and decays at that of γ_2. On the other hand, Eq. (3) describes a more complex situation than Eq. (4). If $(X - \gamma_1) < 0$ and $(X - \gamma_2) > 0$, then Eq. (3) shows a bi-exponential decay as in LE emission. Note that γ_1 and γ_2 represent no direct relationship with each rate constant depicted in Scheme 2. Since the determination of each rate constant was very complex, an iterative fitting method was used to obtain them by developing a macro program in Igor Pro 4.08.

γ_1 and γ_2 correspond to time constants obtained from measured decay curves. To determine each rate constant, we assumed k_D was equal to the inverse of the fluorescence lifetime of **An-*n*-OMe**. Unknown parameters were reduced to 3 terms. In addition, since Eq. (8) was derived from Eqs. (5) to (7), unknown parameters were reduced to two parameters, i.e., k_{CR} is expressed by k_{CS} and k_{-CS}. Furthermore, the validity of Eq. (8) was confirmed from the small dependence of the sum of γ_1 and γ_2 on the monitored wavelength as shown in Table 1.

$$X + Y = \gamma_1 + \gamma_2 = k_D + k_{CS} + k_{CR} + k_{-CS} \quad (8)$$

Fittings were performed by using reconstructed decay curves assuming the excitation pulse as a delta function. As seen from the negligible small residuals of less than 1% between original decay curve and fitted curves, the fitting gave satisfactory results (see Supporting Information, Figs. S5 and S6). The calculated rate constants are shown in Table 1.

k_{CS}, which corresponds to an intramolecular electron transfer process followed by the formation of exciplex from LE, was found to be $5.3 \times 10^8\ s^{-1}$ at 414 nm and $5.1 \times 10^8\ s^{-1}$ at 610 nm for **An-9-G**. While the difference in these two rate constants is very small, k_{-CS} derived at 414 nm is clearly smaller than that at 610 nm. However, using either rate constant, k_{-CS} is obviously smaller than k_{CS}. However, the reverse electron transfer rate has no negligible value and LE is regenerated from the exciplex. Evaluation of the rate constant k_{CS} was performed comparing with anthracene linked to *N*,*N*-dimethylaniline [22]. The charge separation rate constants were determined from fluorescence decay curves due to difficulties in calculation. Considering similar solvent polarity, the rate constant corresponding to k_{CS} was reported to be about $2 \times 10^8\ s^{-1}$, about half of the present result. In addition, anthracene linked to aromatic phenones was reported to have charge separation rate constants of about $2 \times 10^8\ s^{-1}$ [48]. From these comparisons, the obtained k_{CS} values by simulation are plausible. Unfortunately, k_{-CS} was not found in published papers associated with the anthracene moiety. The reason why the k_{CS} of **An-9-G** is be 5 times as large as that of **An-2-G** may originate from the difference of encounter complex between **An-9-G** and **An-2-G** along with free energy changes.

4.5. Fluorescence quantum yields

To evaluate the obtained rate constants assuming the establishment of equilibrium between LE and exciplex, the fluorescence quantum yield of LE involving regeneration from exciplex was calculated. The fluorescence quantum yield of LE, Φ_F, is given by similar treatment of the Förster cycle as follows [49,50]:

$$\Phi_F = \frac{k_F[\mathbf{An^* - n\text{-}G}]}{k_D[\mathbf{An^* - n\text{-}G}] + k_{CR}[(\mathbf{An - n\text{-}G})^*]} \quad (9)$$

where k_F is a radiative rate constant of **An*-*n*-G**. If we apply a steady-state approximation to the concentration of (**An-*n*-G**)*, the following equation is derived:

$$\frac{d[(\mathbf{An - n\text{-}G})^*]}{dt} = k_{CS}[\mathbf{An^* - n\text{-}G}] - (k_{-CS} + k_{CR})[(\mathbf{An - n\text{-}G})^*] = 0$$
$$[(\mathbf{An - n\text{-}G})^*] = \frac{k_{CS}[\mathbf{An^* - n\text{-}G}]}{k_{CR} + k_{-CS}} \quad (10)$$

Eq. (11) is obtained by using Eqs. (9) and (10):

$$\Phi_F = \frac{k_F}{k_D + (k_{CS}k_{CR}/k_{CR} + k_{-CS})} \quad (11)$$

Since the fluorescence quantum yield of **An-*n*-OMe**, Φ_{F0}, is defined as $\Phi_{F0} = k_F/k_D$, which indicates no intramolecular interac-

tion of **An-*n*-OMe**, Φ_F/Φ_{F0} is obtained as follows:

$$\frac{\Phi_F}{\Phi_{F0}} = \left(\frac{k_{CS} k_D^{-1} k_{CR}}{k_{CR} + k_{-CS}} + 1 \right)^{-1} \quad (12)$$

Φ_F/Φ_{F0} corresponds to the fluorescence intensity of **An*-*n*-G** relative to that of **An-*n*-OMe** as shown in Fig. 2, which were determined to be 0.65 and 0.49 for **An-2-G** and **An-9-G**, respectively. Φ_F/Φ_{F0} was also used to calculate the rate constants monitored at 414 nm listed in Table 1: 0.68 and 0.51 for **An-2-G** and **An-9-G**, respectively. If we assume no equilibrium formation between LE and exciplex, the ratios are obtained by the main component of the fluorescence lifetime monitored at 414 nm and k_D: 0.62 and 0.40 for **An-2-G** and **An-9-G**, respectively. These values are lower than those obtained from Fig. 2. To explain the result of fluorescence quenching in Fig. 2, we need to consider the back reaction from exciplex to LE. The small free energy change in exciplex formation can be responsible for the equilibrium establishment in the excited state.

5. Conclusion

In conclusion, the quenching of the excited anthracene moiety of **An-*n*-G** by the guanine moiety results in the formation of an exciplex followed by fluorescence emission. The analyses of fluorescence decay curves gave various rate constants associated with photophysical processes, the validity of which is confirmed by the comparison of the ratio of fluorescence intensity to reference compounds with theoretically obtained ones calculated from rate constants. An equilibrium between LE and exciplex may be established in the excited state, which is responsible for the relatively high intensity of LE emission. The substituent effect on rate constants mainly depends on the reduction potential of **An-*n*-G**. Further work on the sensing ability in vivo are underway in our laboratory.

Acknowledgments

This work was supported by Grants-in-Aid for Scientific Research in a Priority Area "New Frontiers in Photochromism" (Nos. 471 and 19550176) from the Ministry of Education, Culture, Sports, Science, and Technology (MEXT), Japan. We are grateful to Mr. T. Kawai and Dr. M. Ikegami for their support.

Appendix A. Supplementary data

Supplementary data associated with this article can be found, in the online version, at doi:10.1016/j.jphotochem.2010.12.005.

References

[1] B. Armitage, Chem. Rev. 98 (1998) 1171.
[2] J.C. Genereux, J.K. Barton, Chem. Rev. 110 (2010) 1642.
[3] D.B. Hall, R.E. Holmlin, J.K. Barton, Nature 382 (1996) 731.
[4] D. Breslin, G.B. Schuster, J. Am. Chem. Soc. 118 (1996) 2311.
[5] D.A. Dunn, V.H. Lin, I.E. Kochevar, Biochemistry 31 (1992) 11620.
[6] K. Ito, S. Inoue, K. Yamamoto, S. Kawanishi, J. Biol. Chem. 268 (1993) 13221.
[7] I. Saito, M. Takayama, H. Sugiyama, K. Nakatani, A. Tsuchida, M. Yamamoto, J. Am. Chem. Soc. 117 (1995) 6406.
[8] E.D.A. Stemp, M.R. Arkin, J.K. Barton, J. Am. Chem. Soc. 119 (1997) 2921.
[9] S. Delaney, M. Pascaly, P.K. Bhattacharya, K. Han, J.K. Barton, Inorg. Chem. 41 (2002) 1966.
[10] S.E. Evans, S. Mon, R. Singh, L.R. Ryzhkov, V.A. Szalai, Inorg. Chem. 45 (2006) 3124.
[11] B.H. Yun, Y.A. Lee, S.K. Kim, V. Kuzmin, A. Kolbanovskiy, P.C. Dedon, N. Geacintov, V. Shafirovich, J. Am. Chem. Soc. 129 (2007) 9321.
[12] C.E. Crespo-Hernadez, B. Cohen, P.M. Hare, B. Kohler, Chem. Rev. 104 (2004) 1977.
[13] F.D. Lewis, H. Zhu, P. Daublain, B. Cohen, M.R. Wasielewski, Angew. Chem. Int. Ed. 45 (2006) 7982.
[14] K. Kawai, T. Majima, J. Photochem. Photobiol. C 3 (2002) 53.
[15] C.J. Burrows, J.G. Muller, Chem. Rev. 98 (1998) 1109.
[16] T. Kawai, M. Ikegami, T. Arai, Chem. Commun. (2004) 824.
[17] T. Kawai, M. Ikegami, K. Kawai, T. Majima, Y. Nishimura, T. Arai, Chem. Phys. Lett. 407 (2005) 58.
[18] N. Mataga, T. Okada, H. Masuhara, N. Nakashima, Y. Sakata, S. Misumi, J. Luminescence 12 (1976) 159.
[19] T. Okada, T. Saito, N. Mataga, Y. Sakata, S. Misumi, Bull. Chem. Soc. Jpn. 50 (1977) 331.
[20] T. Okada, M. Migita, N. Mataga, Y. Sakata, S. Misumi, J. Am. Chem. Soc. 103 (1981) 4715.
[21] N. Mataga, Pure Appl. Chem. 56 (1984) 1255.
[22] H. Heitele, P. Finckh, S. Weeren, F. Poellinger, M.E. Michel-Beyerle, J. Phys. Chem. 93 (1989) 5173.
[23] J.W. Verhoeven, Pure Appl. Chem. 62 (1990) 1585.
[24] N. Mataga, S. Nishikawa, T. Asahi, T. Okada, J. Phys. Chem. 94 (1990) 1443.
[25] J. Herbich, A. Kapturkiewicz, Chem. Phys. 158 (1991) 143.
[26] Y. Zeng, M.B. Zimmt, J. Phys. Chem. 96 (1992) 8395.
[27] W. Schuddeboom, T. Scherer, J.M. Warman, J.W. Verhoeven, J. Phys. Chem. 97 (1993) 13092.
[28] J.W. Verhoeven, R.J. Willernse, Pure Appl. Chem. 65 (1993) 1717.
[29] I.H.M. van Stokkum, T. Scherer, A.M. Brouwer, J.W. Verhoeven, J. Phys. Chem. 98 (1994) 852.
[30] D.V. Matyushov, G.A. Voth, J. Phys. Chem. A 103 (1999) 10981.
[31] S. Dorairaj, H.J. Kim, J. Phys. Chem. A 106 (2002) 2322.
[32] N. Mataga, H. Chosrowjan, S. Taniguchi, J. Photochem. Photobiol. C 6 (2005) 37.
[33] M.A. Winnik, Acc. Chem. Res. 10 (1977) 173.
[34] M.A. Winnik, Chem. Rev. 81 (1981) 491.
[35] J.B. Birks, Photophysics of Aromatic Molecules, Wiley-Interscience, London, 1970.
[36] Y. Nishimura, M. Kamada, M. Ikegami, R. Nagahata, T. Arai, J. Photochem. Photobiol. A 178 (2006) 150.
[37] I. Ohshiro, M. Ikegami, Y. Shinohara, Y. Nishimura, T. Arai, Bull. Chem. Soc. Jpn. 80 (2007) 747.
[38] F. Babudri, V. Fiandanese, F. Naso, J. Org. Chem. 56 (1991) 6245.
[39] I.B. Berlman, Handbook of Fluorescence Spectra of Aromatic Molecules, Academic Press, New York/London, 1971.
[40] F.D. Lewis, T.L. Kurth, W. Liu, Photochem. Photobiol. Sci. 1 (2002) 30.
[41] Z.R. Grabowski, K. Rotkiewicz, W. Rettig, Chem. Rev. 103 (2003) 3899.
[42] N. Nijegorodov, R. Mabbs, D.P. Winkoun, Spectrochim. Acta A 59 (2003) 595.
[43] M. Migita, T. Okada, N. Mataga, Y. Sakata, S. Misumi, N. Nakashima, K. Yoshihara, Bull. Chem. Soc. Jpn. 54 (1981) 3304.
[44] S. Schneider, H. Rehaber, W. Schübauer, F.D. Lewis, B.A. Yoon, J. Photochem. Photobiol. 99 (1996) 103.
[45] K. Kikuchi, T. Niwa, Y. Takahashi, H. Ikeda, T. Miyashi, M. Hoshi, Chem. Phys. Lett. 173 (1990) 421.
[46] S. Masaki, T. Okada, N. Mataga, Bull. Chem. Soc. Jpn. 49 (1976) 1277.
[47] J.N. Demas, Excited State Lifetime Measurements, Academic Press, New York, 1983.
[48] C. Burgdorff, H.G. Lömannsröen, T. Sander, J. Chem. Soc. Faraday Trans. 92 (1996) 3043.
[49] T. Föster, Z. Elektrochem. 54 (1950) 42.
[50] B. Marciniak, H. Kozubek, S. Paszyc, J. Chem. Educ. 69 (1992) 247.